Assessment of aircraft noise sources variability using an acoustic camera

Mirjam Snellen
Delft University of Technology
Associate professor
Kluyverweg 1, 2629 HS, Delft, the Netherlands.
m.snellen@tudelft.nl
Roberto Merino-Martinez (Delft University of Technology, PhD student)
Dick G. Simons (Delft University of Technology, Full professor)

Noise assessment around airports is hampered due to the observed large variability in noise levels for fly-overs of the same aircraft type, which is not considered by the current models. This paper assumes that the noise variability is due to variations in the aircraft emitted noise, neglecting the effect of the variable atmosphere, as previous work showed that its contribution is maximally 2 dB. In order to quantify and investigate the variability of noise levels during aircraft fly-overs, 115 measurements of noise of landing aircraft were taken using a 32 microphone array. The noise levels from Boeing 737 fly-overs were analyzed and the noise level variability was determined to be approximately 16 dB. After determining the engine settings from the spectrograms, it was found that variations on the engine settings explain over 55% of the observed total noise variation. In addition, by performing beamforming on the acoustic data, it was confirmed that airframe noise (from the landing gear and deployed flaps) is dominant for several frequencies, especially for modern aircraft.

NOMENCLATURE

α=Atmospheric absorption coefficient.
$\Delta t_{j,n}$= Time delay between the n^{th} microphone and the j^{th} grid point, [s].
θ= Angle between the relative position vector of the source with respect to the observer and the source speed vector
$\vec{\xi}_j$=Vector pointing at the j^{th} grid point of the scan plane, [m].
A=Source autopower, [dB].
B=Number of fan blades.
BPF=Blade Passing Frequency, [Hz].
$\boldsymbol{C}$=Cross Spectral Matrix, [Pa²].
f=Emitted frequency, [Hz].
f'=Observed frequency, [Hz].
$\vec{g}_j$=Steering vector at the grid point $\vec{\xi}_j$.
$\vec{M}$=Mach vector.
n=Fan rotational speed, [rpm]
N =number of microphones in the array.
$N1\%$=Fan rpm percentage with respect to the maximum fan rotational speed, [%].
p=Atmospheric pressure [Pa].
$\vec{p}$=Vector with the Fourier-transformed recorded pressures in each microphone.
$\vec{r}_{j,n}$=Distance vector between the n^{th} microphone and the j^{th} grid point, [m].
RH=Relative humidity, [%].
T=Temperature, [K].
$\vec{v}$=Velocity vector of the source, [m/s].
$\vec{x}_n$=Position vector of the n^{th} microphone, [m].

1 INTRODUCTION

Noise pollution has been a great nuisance for residents living in the vicinity of airports for decades. Even though there have been large reductions in the noise produced by individual aircraft over the years, the continuously growing air traffic and stricter noise regulations have caused that aircraft noise is currently one of the main issues the industry has to deal with. In fact, noise restrictions are nowadays the limiting factor for increasing the capacity of many airports.

Aircraft engine noise has decreased remarkably on modern aircraft, since high bypass ratio turbofan engines were implemented around the 1970s. This fact causes that engine noise is not always dominant anymore and airframe noise, which is produced by the interaction of the aerodynamic surfaces and the surrounding turbulent flow [1], becomes relevant, reaching similar Sound Pressure Levels (SPL) as the engine noise in certain conditions, especially during landing. In order to further reduce the generated noise emissions, it is essential to determine which elements of the aircraft contribute to the total noise and their relative importance.

In addition, most airports use models to calculate aircraft noise levels which employ the so-called Noise-Power-Distance (NPD) tables, such as INM [2-6]. These tables contain SPLs at predefined distances for different aircraft and flight procedures, based on information provided by the aircraft manufacturers. This method estimates approximated fixed values, obtaining a unique noise level for a certain aircraft type, flight phase and location. However, experimental measurements confirm that variations as large as 12 dB can be observed for the same aircraft type, flight phase and location [7,8]. This variability is assumed to be due to the effect of the variable atmosphere and the variations of the emitted noise at the source. Aircraft noise depends on several parameters such as the engine settings, aircraft velocity and flight configuration, which are not fully taken into account by the NPD tables. The atmospheric propagation conditions are taken into account by the NPD tables only in an average sense.

Microphone arrays, also known as acoustic cameras, are a very useful tool for localizing acoustic sources in flying aircraft. These devices consist of a considerably large amount of microphones located in a certain pattern. By post-processing the recorded data with a beamforming algorithm, acoustic images, which show the estimated location and SPL of the signal of interest, can be obtained.

In order to localize the main contributors to aircraft noise and assess the noise levels variability, an experimental measurement campaign was performed next to Amsterdam Airport Schiphol with a 32 microphone array which recorded the data of 115 fly-overs during the approach stage. This airport was selected due to its high number of flights (over 1000 air transport movements per day). The aircraft trajectories and engine settings will be estimated to enable this analysis. This paper intends to follow the research presented by Simons *et al.* in [7], extending the amount of fly-overs measured.

Section 2 is devoted to the beamforming principles and section 3 briefly explains the experimental set-up. The methods used to predict the aircraft engine settings are introduced in section 4. Finally the results are gathered in section 5 and the conclusions drawn are presented in section 6.

2 BEAMFORMING PRINCIPLES

As previously mentioned, by using a beamforming algorithm on the data acquired by the acoustic array the location and SPL of a signal of interest can be determined. Beamforming methods are increasingly being employed in the aerospace industry to develop efficient noise control strategies. These methods assume a certain source model (usually a monopole) and they work in the frequency domain.

2.1 Data pre-processing

In the case of fly-over measurements, several corrections need to be made to the acoustic data before using a beamforming algorithm on it. For performing all these corrections, the aircraft flight paths have to be precisely estimated, as will be explained in section 3.
First of all, the background noise needs taken into account, such as the noise generated by the microphone array electronics or the ambient noise. Therefore, all the SPL values under a threshold value of 30 dB (typical SPL in a library) were neglected.

Afterwards the Doppler effect due to the relative movement of the aircraft with respect to the observer needs to be considered [9].

$$\frac{f'}{f} = \frac{1}{1 - \left\|\vec{M}\right\| \cos(\theta)} \tag{1}$$

Equation (1) determines the frequency shift due to the Doppler effect, where f' is the observed frequency, f is the emitted frequency, $\vec{M} = \vec{v}/c$ is the Mach vector, i.e., the velocity vector, $\vec{v}$, divided by the sound speed, c, and θ is the angle between the relative position vector of the source with respect to the observer and the source speed vector. The last two parameters are known from the aircraft trajectory estimation performed in section 3. This effect can be observed in the bended curves of the engine tones, see figure 1. The effect of the moving source also affects the beamforming algorithm, as it will be commented in subsection 2.2.

The propagation effects have to be taken into account for obtaining the actual results at the source [10,11]. Equation (2) shows how to estimate the SPL at the source, namely at a distance of 1 metre, adding to the sound recorded at the observer position the transmission losses due to geometrical spreading and the atmospheric attenuation at a distance r.

$$SPL(1m) = SPL(r) + 20\log_{10}(r) + \alpha r + DI(\theta) \tag{2}$$

The atmospheric absorption coefficient, α, depends mostly on the frequency, temperature, relative humidity and atmospheric static pressure. The last term in equation (2) is a directivity function that depends on θ.

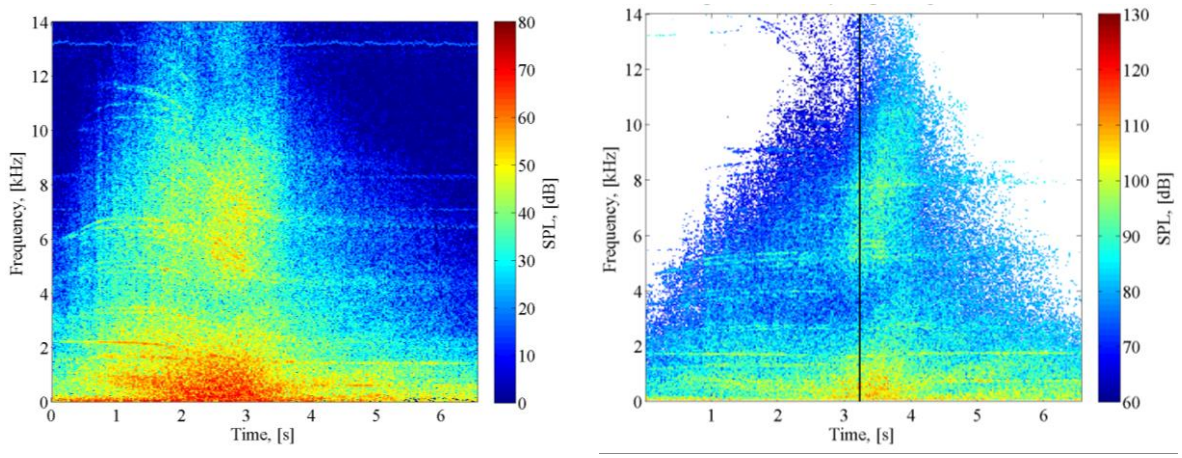

Figure 1: **The spectrogram on the left is the sound recorded by a single microphone in the array during a flyover. After correcting for the background noise and the Doppler and propagation effects, the spectrogram on the right is obtained, which represents the sound at the source. The black line shows the time overhead. Note the different decibel scales.**

The result of all the mentioned corrections is depicted in figure 1 in the form of two spectrograms (note the different decibel colour scale).

2.2 Conventional Frequency Domain Beamforming (CFDBF)

The so-called Conventional Beamforming or delay-and-sum beamforming is probably the simplest and most robust beamforming algorithm and, therefore, it is the most widely used method in aeroacoustic experiments. This technique is based on the phase delays between the emission of the sound signal at the source (each scan point of the scan plane considered) and the received signal at each microphone [13-17]. This method can be employed either in the time domain or in the frequency domain, by applying a discrete Fourier transform to the data. The latter is widely used due to the lower computational time required and possibility of performing a frequency analysis.

If an array with *N* microphones located at $\vec{x}_n = (x_n, y_n, z_n) \in \mathbb{R}^{Nx3},\ n = 1 \dots N,$ is considered, the steering vectors $\vec{g}_j \in \mathbb{C}^{Nx1}$ determine the source description at each grid point $\vec{\xi}_j$ in the scan plane analysed. Each steering vector has *N* components $g_{j,n},\ n = 1 \dots N$ which are the estimated pressure amplitudes at the microphone locations of an ideal source at grid point $\vec{\xi}_j$ with unit strength [14].

$$g_{j,n} = \frac{-e^{-2\pi i f \Delta t_{j,n}}}{4\pi r_{j,n}\left(1 - \left\|\vec{M}\right\|\cos\theta\right)^2} \tag{3}$$

where $\Delta t_{j,n}$ and $r_{j,n}$ are the time delay and distance between grid point $\vec{\xi}_j$ and the n^{th} microphone, respectively. For a general case with a moving source [14], these two variables are defined in equations (4) and (5), where β is a parameter defined as $\beta = \sqrt{1 - \left\|\vec{M}\right\|^2}$.

$$\Delta t_{j,n} = \frac{-\vec{M}\cdot\left(\vec{x}_n - \vec{\xi}_j\right) + \sqrt{\left(\vec{M}\cdot\left(\vec{x}_n - \vec{\xi}_j\right)\right)^2 + \beta^2\left\|\vec{x}_n - \vec{\xi}_j\right\|^2}}{c\beta^2} \tag{4}$$

$$r_{j,n} = \left\|\vec{x}_n - \vec{\xi}_j\right\| \tag{5}$$

The expressions for a static source are obtained for $\vec{M} = \vec{0}$ and $\beta = 1$, respectively. The Conventional Frequency Domain Beamforming algorithm (CFDBF) works with the Fourier-transform of the recorded pressure amplitudes in each of the *N* microphones of the array as a complex vector $\vec{p}(f) \in \mathbb{C}^{Nx1}$ dependent on the frequency f:

$$\vec{p}(f) = \begin{pmatrix} p_1(f) \\ \vdots \\ p_N(f) \end{pmatrix} \tag{6}$$

After performing a least squares minimization of the difference between the recorded pressures vector $\vec{p}$ and the estimated amplitude of the source vector, $a\vec{g}_j$, the source autopower, A, obtained for a grid point $\vec{\xi}_j$ is determined to be [14]:

$$A\left(\vec{\xi}_j\right) = \frac{1}{2}\frac{\vec{g}_j^* \vec{p}\vec{p}^* \vec{g}_j}{\|\vec{g}_j\|^4} = \frac{\vec{g}_j^* \boldsymbol{C} \vec{g}_j}{\|\vec{g}_j\|^4} \quad (7)$$

In equation (7) an asterisk $(\cdot)^*$ denotes complex conjugation and $\boldsymbol{C}$ is the NxN Cross Spectral Matrix (CSM) defined as one half of the product of vector $\vec{p}$ and its complex conjugate. After obtaining the values of the source's autopowers for each grid point, beamforming plots are obtained.

3 EXPERIMENTAL SET-UP

In order to gather a representative amount of data, 115 fly-over measurements were recorded at Amsterdam Airport Schiphol using an acoustic camera which consists of 32 microphones. The array shape is flexible due to the 1350 holes drilled for placing the microphones on the wooden plates. For this research they were placed following a spiral distribution, as it can be seen in figure 2. This array configuration has an effective diameter of 1.7 m and it was chosen due to its varying microphone spacing, which provides good results over a wide range of frequencies with a relatively small amount of sidelobes [18]. The microphone array uses filters for obtaining a frequency range from 45 Hz to 11,200 Hz and the sample frequency employed was 40 kHz, i.e. higher than the Nyquist rate. Moreover, an optical camera was attached in the centre of the array facing straight up from the ground, which takes pictures with a synchronised time reference with the microphones.

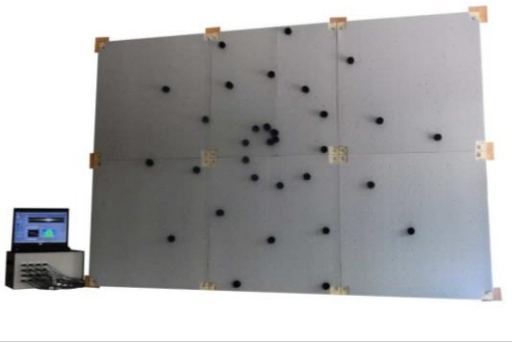

Figure 2: 32 Microphone array configuration in a spiral distribution.

Figure 3: Experimental set-up located 1240 m to the South of the threshold of the Aalsmeerbaan (36R) Schiphol airport runway.

	June 18th 2013	August 8th 2013
Temperature	27.2ºC	20.3ºC
Humidity	56%	61%
Air pressure	101,500 Pa	101,890 Pa
Precipitation	0 mm	0 mm
Wind speed (at 10 m height)	2 m/s	5 m/s
Wind direction (at 10 m height)	160º	340º

Table 1: Meteorological conditions at Amsterdam Airport Schiphol at 12:00.

Flight trajectories during landing are typically more regular than the ones for take-off, since all aircraft follow the Instrument Landing System (ILS) approach. Moreover, the main reason for recording landing aircraft is because the engines are usually operating at idle and the high lift devices and landing gear are deployed. Therefore, the engine noise is less dominant and other noise sources, such as airframe noise, are more likely to be identified. Hence, the acoustic camera was placed 1,240 meters to the South of the threshold of the Aalsmeerbaan Schiphol airport runway (36R), mainly used for landing, as illustrated in figure 3.

Henceforth, the data will be referred to the distances to the array, with the Y axis in the direction of the runway and the X axis perpendicular to it. The measurements were taken on two different days with similar weather conditions and low wind speeds. Table 1 gathers the most important meteorological data for those days at 12:00, as obtained from the Royal Netherlands Meteorological Institute, KNMI [12]. The same parameters are provided every hour.

The recorded acoustic data correspond to 21 different aircraft types gathered in 12 different aircraft families, from which the Boeing 737 is the most numerous model with 59 measurements available.

As stated before, in order to be able to properly model the propagation and the Doppler effects, the trajectories of the aircraft need to be precisely determined and synchronised with the acoustic and optical data. Most aircraft have a similar flight path when approaching the runway, but variations in the velocity usually occur.

Three different approaches were used to determine the position and velocity of the aircraft, each of them uses data from a different source: The ADS-B (Automatic Dependent Surveillance-Broadcast), the ground radar from Air Traffic Control and the extrapolation of the optical camera images.

The agreement between the three methods is very satisfactory. The optical camera data is preferred because of its versatility and availability and because it is easier to overlay the beamforming results to the optical frames. The other methods were used as a validation tool for the trajectory estimations. The average flight height and average aircraft velocity at the acoustic camera position, i.e. overhead, were determined to be 67 m and 271 km/h, respectively.

4 DETERMINATION OF THE ENGINE SETTINGS

Once the pre-processing corrections have been applied to the data, an analysis of the fan engine settings of each aircraft can be performed with the help of the spectrograms, as depicted in figure 4 for an example of a Boeing 737-800.

The aim of this analysis is to determine the Blade Passing Frequency (BPF) of each fly-over, in order to calculate the specific fan engine settings, as seen in equation (8). Since part of the fan noise, which is generated by the interaction between the fan blades and the stator vanes, is tonal, there will probably be also higher harmonics present in the spectrum.

$$BPF = f_1 = \frac{B\,n}{60} \tag{8}$$

These harmonics are multiples of the BPF:

$$f_k = k\,f_1, \qquad k = 1,\ 2,\ 3... \tag{9}$$

In equation (8), B is the number of fan blades, f_1 is the BPF, also known as first harmonic tone, and n is the fan rotational speed measured in rpm. In order to work with non-dimensional variables, the fan rotational speed, n, can be divided by the maximum fan rotational speed, n_{max}, to obtain the fan rpm percentage, also known as N1% as it refers to the low pressure spool.

However, determining the BPF is not always an easy task due to possible changes by the pilot in the engine settings during landing. Hence a study of the forward arc spectra (the sound when the aircraft is approaching the array) is recommended since the fan noise is dominant in that direction, due to the aircraft noise directivity [10]. In figure 4 the solid black line represents the overhead time and the dashed black lines show the time bin selected for this case.

After extracting a time interval from the spectrogram, it is averaged over time and a 10^{th} degree polynomial is fitted to the averaged spectrum, modelling the broadband noise, see figure 5. This curve is subtracted from the data and the difference is then squared in order to only consider positive amplitudes and observe the engine tonal peaks more clearly. This magnitude is called the squared residual vector and is illustrated in figures 6 and 7.

Once all the peaks of interest (higher than a minimum amplitude) have been localized in the tonal spectra, three different methods are employed, in order to determine the engine settings of each measurement:

1. Method 1 considers all the possible combinations of three peaks for all the peaks using a least squares approach and estimating a BPF value for each case. The four combinations with the smallest deviation between the modelled and measured peaks are selected as possible candidates for harmonics of the BPF, as depicted in figure 6.

2. Method 2 uses the three peaks with the lowest frequency and the differences between the location of the peaks as potential candidates for the BPF. The selected BPF value is the one which explains the tones in a better way as long as it is a realistic value.

3. Method 3 employs a synthetic noise model for the full expected spectrum, including an approximation for the airframe tones. An iterative process is performed varying the engine setting N1% within a sensible range, i.e. the BPF value. The engine setting resulting in a maximum correlation between the modelled and the experimental data is selected as the candidate, as shown in figure 7.

The spectrograms need to be individually studied with great care, and the outcomes of the three methods are evaluated depending on their agreement with the spectra. Even if the three methods usually provide similar results, it is required to confirm whether the solution has a realistic value and explains as many tones as possible.

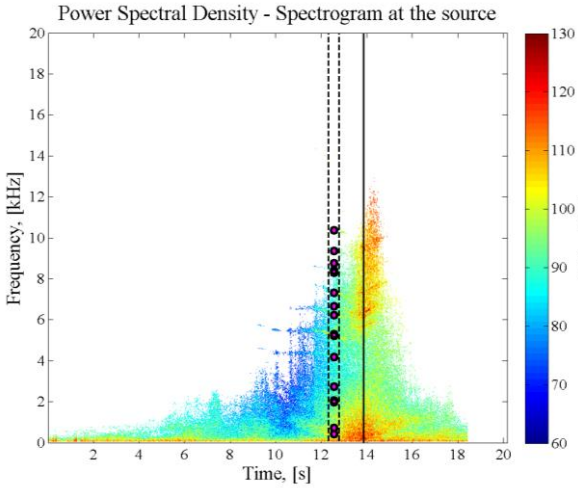

Figure 4: Time window selected in the spectrograms (dashed lines) and peaks selected (circles).

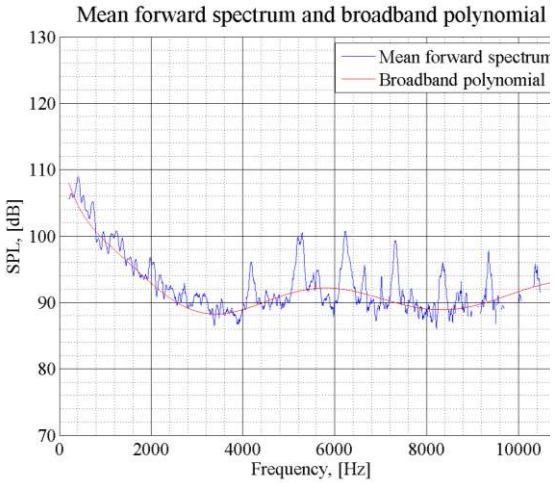

Figure 5: Mean forward spectrum and 10^{th} degree broadband polynomial.

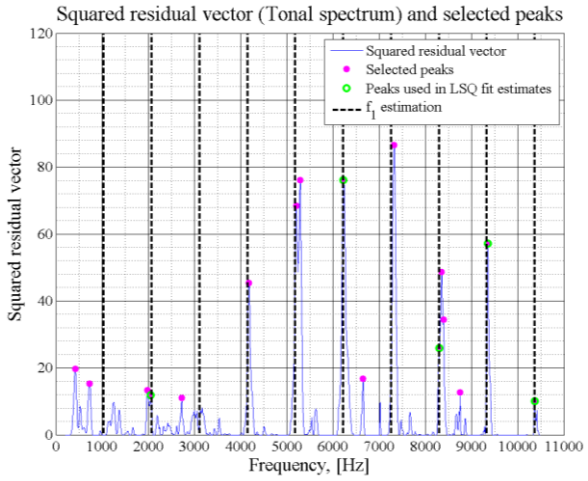

Figure 6: BPF (f_1) estimation based on the peaks for the 1st method.

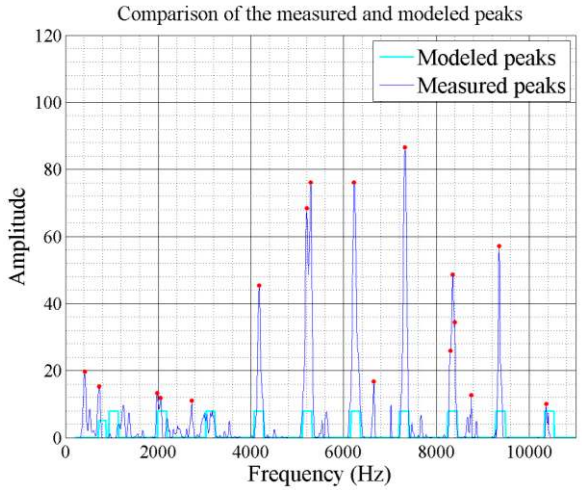

Figure 7: Squared residual vector and the selected peaks from figure 4 with the modelled peaks (3rd method).

The found engine settings (N1%) range in this research varies from 40% to 70%, which are typical values for commercial planes during the landing stage.

5 RESULTS

5.1 Aircraft noise variability

First of all, the variability in the noise levels due to atmospheric changes was neglected in this research since the measurements took place in two days with very similar meteorological conditions. Also, previous studies [7,8] showed that this variability is typically less than 2 dB for the distances considered.

Since the Boeing 737 family was the most numerous during the measurement campaign, the noise variability analysis for this aircraft type is presented in this paper, specifically the series 700, 800 and 900, which are 47 out of the 59 Boeing 737 measurements. All the measured aircraft from these series use a CFMI CFM56-7B high-bypass turbofan engine which has 24 fan blades and a maximum fan rotational speed of n_{max} = 5175 rpm. Using the methods explained in section 4 and equation (8) the fan rotational speed of each measurement can be calculated and divided by n_{max} in order to obtain the engine settings, N1%.

Two different noise metrics were employed for this study: the maximum Overall SPL (OSPL) at the source and the Sound Exposure Level (SEL or LAE). The OSPL at the source was calculated considering the propagation loss explained in equation (2). The SEL takes into account the effect of duration by integrating the measured OSPL at the array with respect to the time. The integration limits are determined by the closest point at each side of the maximum OSPL which have a OSPL 10 dB lower than the maximum OSPL. A comparison of the different correlations between these metrics and the engine settings and the aircraft velocity is presented in figures 8 and 9, respectively.

In addition, the correlation coefficients, ρ, the coefficients of determination, ρ^2, and the p-values are calculated and depicted in each plot. A linear least squares fit is also included in each case.

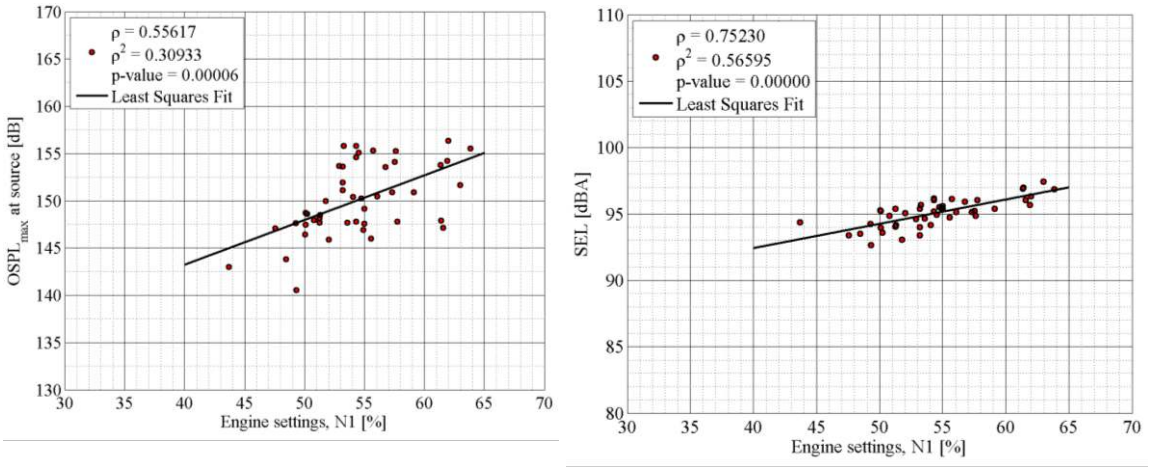

Figure 8: Correlation between the maximum OSPL (left) and the SEL and the engine settings (N1%) for the Boeing 737 (series 700, 800, 900) case. A linear least squares fit is also included.

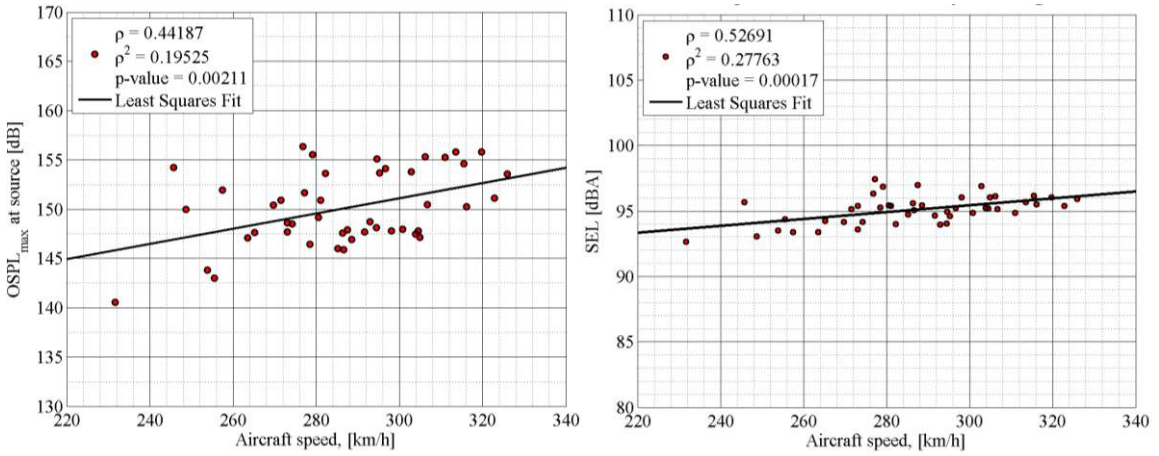

Figure 9: Correlation between the maximum OSPL (left) and the SEL and the aircraft velocity for the Boeing 737 (series 700, 800, 900) case. A linear least squares fit is also included.

As it can be observed in the plots above, there is a relatively strong correlation in all cases, especially with the engine settings. The p-value is a measure of significance of the found correlation and expresses the possibility to obtain this correlation coefficient when the variables are uncorrelated, therefore it should be as low as possible. In these four examples the p-values are considerably lower than the typical threshold value of 0.05 [7]. This means that the correlations found are significant.

The coefficient of determination, ρ^2, expresses the fraction of the variance in the two variables that is shared. For instance in the case of the SEL vs the engine settings, $\rho^2 \approx 0.57$, then 57% of the total variance observed in the SEL can be explained by the variation in the fan rotational speed.

The correlation coefficient in the case of the SEL is significantly higher than the one found for the maximum OSPL data. This is probably due to the fact that the SEL metric takes into account the duration of the noise, while the maximum OSPL just considers the maximum value during the fly-over. Therefore, the SEL metric offers a more averaged value compared to the singular value of the maximum OSPL.

In this research a variability of approximately 16 dB is found for the maximum OSPL and of 5 dBA for the SEL for the same aircraft type (see figures 8 and 9).

5.2 Beamforming analysis

For this research the Conventional Frequency Domain Beamforming algorithm was applied to the acoustic data recorded by the 32 microphones of the array and the resulting beamforming plots were overlaid on the images taken by the optical camera.

Figures 8 and 9 illustrate the results of the beamforming analysis for an Airbus A321 at 1719 Hz and a Boeing B777-W at 1293 Hz. In the first case (figure 10) there is a clear noise source at the nose landing gear of 130 dB. In the second case (figure 11) two different sources can be observed: a 140 dB source on the nose landing gear and a larger source of 143 dB from what appears to be a combination of the main landing gear and the deployed flaps.

These source plots confirm the importance of the airframe noise, especially in modern aircraft and at frequencies up to around 3000 Hz. Other measurements of the same aircraft types as those depicted here also showed similar noise sources at these frequencies.

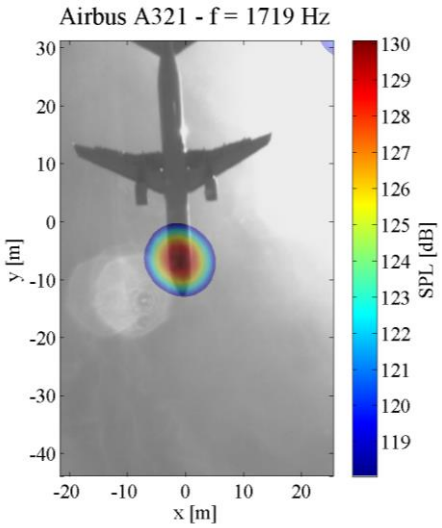

Figure 10: Beamforming source plot for an Airbus A321 at 1719 Hz.

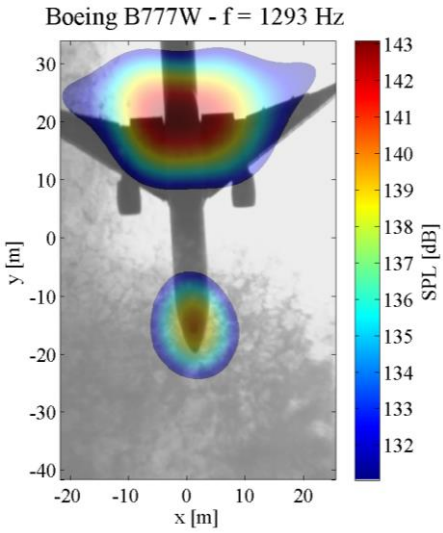

Figure 11: Beamforming source plot for an Boeing B777-W at 1293 Hz.

6 CONCLUSIONS

In this paper the issue of noise variability for aircraft observed directly under the flight path was analyzed. The sound pressure level variations for the same aircraft type can be as large as 16 dB, hence posing a problem when assessing the noise levels around airports and enforcing environmental laws. The noise assessment models usually employ Noise-Power-Distance tables, which do not consider these variations and only provide fixed values of actual aircraft noise levels. In this research, the noise variability was assumed to mostly depend on the emitted noise at the source, i.e. the aircraft itself, neglecting the effect of a variable atmosphere.

Noise levels from landing aircraft were recorded in a full scale field experiment using a 32 microphone acoustic camera at Schiphol airport. After correcting the data taking into account propagation effects, Doppler effect and background noise, the engine settings were determined by analyzing the typical tonal peaks from the fan noise.

The total variability observed directly under the flight path was approximately 16 dB for several landings of the same aircraft type (Boeing 737, series 700, 800 and 900). A correlation analysis showed that both the maximum OSPL measured and the SEL are highly related to the fan rotational speed of the turbofan engines and the aircraft speed. Correlation coefficients of around 0.75 are obtained for variation of the SEL with the engine settings, meaning that more than 55% of the total observed variation can be explained by changes in the engine settings. The aircraft velocity, on the other hand, had lower correlation values, but still explains more than 20% of the total variation observed.

The acoustic camera provides beamforming source plots, also known as acoustic images, which give information about the noise source's location on the aircraft. After using the Conventional Frequency Domain Beamforming it was determined that the airframe noise generated by the landing gear and by the deployed flaps is the dominant source for certain frequencies, especially for modern aircraft. Future work may relate the SPL values from the beamforming plots to the fan harmonics frequencies, which would probably lead to higher correlation values with the engine settings.

In conclusion, in order to solve the issue of airport noise assessment due to the large noise level variations, it is highly recommended to include more accurate aircraft engine setting data into the models for noise contour calculations around airports.

REFERENCES

[1] Lighthill, M.J., "On sound generated aerodynamically, I. General theory," Proc. R. Soc. London Ser. A 221, pp 564-587. 1952.
[2] SAE, Procedure for the Calculation of Airplane Noise in the Vicinity of Airports, Aerospace Information Report AIR 1845, prepared by the SAE A-21 Committee on Aircraft Noise, Society of Automotive Engineers, Inc., 400 Commonwealth Drive, Warrendale, PA 15096, January 1986.
[3] ICAO Circular 205-AN/1/25, Recommended method for computing noise contours around airports, International Civil Aviation Organization (ICAO), Montreal, Canada, 1988.
[4] ECAC.CEAC Doc 29, Report on Standard method of Computing Noise Contours around Civil Airports, Volume 1&2, 3rd Edition, 2005.
[5] He, B., Dinges, E., Hemann, J., Rickel, D., Mirsky, L., Roof, C.J., Boeker, E.R., Gerbi, P.J. and Senzig, D., "Integrated Noise Model (INM)" Version 7.0 User's Guide, Report No. FAA-AEE-07-04, Federal Aviation Administration (FAA), U.S. Department of Transportation, Washington, DC, April 2007.
[6] Boeker, E.R., Dinges, E., He, B., Fleming, G.G., Roof, C.J., Gerbi, P.J., Rapoza, A.S. and Hemann, J., "Integrated Noise Model (INM)" Version 7.0 Technical Manual, Report No. FAA-AEE-08-01, Federal Aviation Administration (FAA), U.S. Department of Transportation, Washington, DC, January 2008.
[7] Simons, D., Snellen, M., Midden, B., Arntzen, M. and Bergmans D.H.T., "Assessment of noise level variations of aircraft fly-overs using acoustic arrays," Paper accepted for publication in the Journal of Aircraft.
[8] Bergmans, D., Arntzen, M. and Lammen, W., "Noise attenuation directly under the flight path," National Aerospace Laboratory (NLR), Report nº NLR-TP-2011-262. November 2011.
[9] Howell, G.P., Bradley, A.J., McCormick M.A. and Brown J.D., "De-Dopplerization and acoustic imaging of aircraft flyover noise measurements," Journal of Sound and Vibration, No. 105, pp 151-167. 1986.

[10] Arntzen, M., "Aircraft noise calculation and synthesis in a non-standard atmosphere," PhD thesis, Delft University of Technology. December 2014.
[11] Ruijgrok, G.J.J., Elements of aviation acoustics. Second edition 2007. VSSD. Delft, The Netherlands. ISBN-10 90-6562-155-5.
[12] Royal Netherlands Meteorological Institute (KNMI) website. Uurgegevens van het weer in Nederland. [Accesed in August 2013]. URL http://www.knmi.nl/klimatologie/uurgegevens/
[13] Siller, H.A., "Localisation of sound sources on aircraft in flight," Berlin Beamforming Conference, BeBeC 2012-01, 2012.
[14] Sijtsma, P., "Phased array beamforming applied to wind tunnel and fly-over tests," National Aerospace Laboratory (NLR), Report nº NLR-TP-2010-547. December 2010.
[15] Sijtsma, P. and Stoker, R.W., "Determination of Absolute Contributions of Aircraft Noise Components using Fly-Over Array Measurements," AIAA Paper 2004-2958. 2004.
[16] Sitjsma, P. and van der Wal, H.M.M., "Identification of Noise Sources on Civil Aircraft in Approach using a Phased Array of Microphones," National Aerospace Laboratory (NLR), NLR-TP-2004-166. April 2004.
[17] Michel, U., Barsikow, B., Helbig, J., Hellmig, M. and Schüttpelz, M., "Flyover noise measurements on landing aircraft with a microphone array," AIAA Paper 1998-2336. 1998.
[18] Goot, R. van der, Hendriks, J., Scheper, K., Hermans, G., Wal, W. van der and Simons D.G., "A low cost, high resolution acoustic camera with a flexible microphone configuration," Berlin Beamforming Conference, BeBeC 2012-08, 2012.